White Rose Research Online

eprints@whiterose.ac.uk
https://eprints.whiterose.ac.uk
Universities of Leeds, Sheffield and York

Deposited via The University of Leeds.

White Rose Research Online URL for this paper:
https://eprints.whiterose.ac.uk/id/eprint/166280/

Version: Accepted Version

Article:
Mortimer, LF and Fairweather, M (2020) Density ratio effects on the topology of coherent turbulent structures in two-way coupled particle-laden channel flows. Physics of Fluids, 32 (10). 103302. p. 103302. ISSN: 1070-6631

https://doi.org/10.1063/5.0017458

© 2020 Author(s). This article may be downloaded for personal use only. Any other use requires prior permission of the author and AIP Publishing. This article appeared in Mortimer, LF and Fairweather, M (2020) Density ratio effects on the topology of coherent turbulent structures in two-way coupled particle-laden channel flows. Physics of Fluids, 32 (10). 103302 and may be found at https://doi.org/10.1063/5.0017458.

Reuse
Items deposited in White Rose Research Online are protected by copyright, with all rights reserved unless indicated otherwise. They may be downloaded and/or printed for private study, or other acts as permitted by national copyright laws. The publisher or other rights holders may allow further reproduction and re-use of the full text version. This is indicated by the licence information on the White Rose Research Online record for the item.

Takedown
If you consider content in White Rose Research Online to be in breach of UK law, please notify us by emailing eprints@whiterose.ac.uk including the URL of the record and the reason for the withdrawal request.

UNIVERSITY OF LEEDS
University of Sheffield
UNIVERSITY of York

Density ratio effects on the topology of coherent turbulent structures in two-way coupled particle-laden channel flows

L. F. Mortimer [a)] and M. Fairweather

School of Chemical and Process Engineering, University of Leeds, Leeds, LS2 9JT, UK

[a)] *Corresponding author: l.f.mortimer@leeds.ac.uk*

This investigation considers the effect of density ratio on the modification of coherent turbulent structures in particle-laden channel flows at shear Reynolds number, $Re_\tau = 180$. Direct numerical simulation and Lagrangian particle tracking are used to accurately predict the motion of particles dispersed within the flow at three Stokes numbers, $St^+ = 0.1, 50$ and 92. Particle-fluid coupling is achieved through a local element-based force feedback field in the Navier-Stokes equations, which are solved using a 7th-order accurate spectral element method. After an initial transitory period wherein the effects of particle-fluid interaction are emphasized, the low density ratio particles are found to enhance the turbulence field, increasing the frequency of Q-criterion satisfying regions, while the inertial particles suppress the turbulence, reducing the number of quasistreamwise vortices. Results indicate that the topology of the quasistreamwise vortices are altered by the presence of the particles in the viscous sublayer, the buffer layer and the log-law region such that the distribution of the third invariant of the deviatoric tensor, R, is widened by the presence of tracer-like particles and made thinner by the inertial particles. This effect reduces the amount of unstable focus / compressing regions and stable focus / stretching regions which account for the streamwise vortical structures observed in these types of flow. Investigating the instantaneous coupling force field surrounding turbulent structures and low speed streaks shows that particles exert their greatest influence on the fluid in the regions noted, and mechanisms by which the particulate phase interacts with turbulent vortices are analysed.

I. INTRODUCTION

The temporal evolution of the spatial distribution of particles in transportive multiphase flows is of great interest in many applications such as airborne disease transmission (Zhang and Chen, 2007), aerodynamics in extreme weather conditions (Wu and Cao, 2016) and chemical mixing processes (Pukkella et al., 2019). In such applications, particle inertia plays a dominant role in the resultant migratory and interaction behaviour of particles, as those with certain properties have been observed to avoid regions of vortical intensity in favour of those with increased strain rate. Outside of the dilute regime, however, vortical structures which form and dissipate dynamically close to wall boundaries are modulated by the presence of particles, thereby modifying the dispersive properties and particle concentration profiles in those regions. This has important consequences for the prediction of those locations where dense populations of particles are likely to occur, which is of interest when considering erosion by particles, and particle deposition and agglomeration. Furthermore, advantageous behaviour such as turbulent drag reduction can be achieved through careful use of such solid particle additives in a similar manner, which until recently was only achievable through the addition of specifically manufactured polymers (Ptasinski et al., 2003; Lumley, 1973). The generation of such knowledge is also of interest to higher level techniques such as the two-fluid Eulerian-Eulerian model which can be improved with better understanding of the mechanisms by which momentum is exchanged between the two phases.

Early experiments performed in wall-bounded geometries (Zisselmar and Molerus, 1979; Tsuji et al., 1984; Kulick et al., 1994; Rogers and Eaton, 1991) indicated both substantial turbulence enhancement and attenuation dependent upon the system parameters. Due to the nature of the modulation mechanisms, which act over a large range of length and timescales and are clearly very parameter-sensitive, it is difficult to develop understanding by studying solely experimental findings. Modern high accuracy computational fluid dynamic techniques allow turbulent systems to be probed nonintrusively on various scales, and as such have provided a useful tool in recent years in studying such phenomena. Initial studies have been performed in turbulent systems over the last few decades to ascertain to what extent each parameter influences this interaction between the particles and the turbulence field. Gore and Crowe (1989) indicated the critical parameter to be the ratio of the solid particle diameter to the integral length scale of the fluid, d_P/L. Elghobashi (Elghobashi, 1994; Elghobashi, 2007) further generalized this classification behaviour based on the Stokes number using the Kolmogorov time scale, St_K, as well as on the solid-fluid volume fraction, introducing the influence of density ratio. Both of these parameters strongly indicate that the degree of coupling impact is related to the ratio of the length and timescales between the particulate and fluid phases.

For increased volume fractions, the method by which particle-laden flows are simulated needs to be amended to account for the momentum feedback from the particles to the fluid (Elghobashi, 1991). This entails various complexities which must be addressed in order to obtain an accurate representation of this process. Firstly, the particle force-balance equation terms all require knowledge of the undisturbed fluid velocity at the particle centre point, which is not an issue for one-way coupled flows. However, with particle-fluid coupling, there are inherent modifications to the fluid velocity due to the presence of the particles. A resolution to this issue was posed by Boivin et al. (2000) who argued that if the particle diameter is smaller than the numerical grid spacing, then the disturbed and undisturbed velocities will be sufficiently similar. For point-particle direct numerical simulation techniques, we already ensure that the particle diameter is less than the Kolmogorov length scale, which is on the order of the minimum grid spacing. Therefore, this issue is usually resolved by default. Secondly, particle forces exerted on the fluid are represented by a Dirac delta function, in that they apply a localized force onto the surrounding fluid. In practice, the total force from all particles within an Eulerian cell is attributed to the momentum feedback term when solving for that cell's updated velocity. This is referred to as the particle-source-in-cell (PSIC) method and has been shown in recent years to produce convincing results (Ferrante and Elghobashi, 2003; Zhao et al., 2015), so long as the particle size remains lower than the smallest flow length scales and the forcing field remains smooth (Eaton, 2009). Both requirements will be demonstrated to be satisfied within the present study.

Recent work simulating densely dispersed flows can be divided into two main categories relating to the system considered; homogeneous isotropic turbulence (HIT) and wall bounded turbulence. Boivin et al. (1998) studied the former for sustained HIT, focusing on the effect of mass loading on turbulence properties. It was observed that the turbulence kinetic energy and its dissipation rate were dampened as the mass loading was increased. Furthermore, for small particles, the small-scale portion of the energy spectrum was increased. Similar studies have been performed in decaying turbulence (Ferrante and Elghobashi, 2003; Abdelsamie and Lee, 2012) which further indicated that small particles enhance the turbulence kinetic energy and dissipation rate whilst large particles decrease them. Midrange particles with Stokes numbers close to unity (based on the Kolmogorov timescale) exhibited very little effect. More recently, Luo et al. (2017) used an immersed boundaries technique to study direct numerical simulations of particle-laden decaying isotropic turbulence. The particles

considered were highly inertial (with diameters 25 times the Kolmogorov length scale). Turbulence was found to be enhanced by heavy particles, but suppressed by light particles, indicating a lack of diameter influence at such scales.

Pan and Banerjee (1996) performed two-way coupled particle-laden turbulent channel flow simulations at $\phi_P = 4 \times 10^{-4}$. Preferential accumulation of particles in low-speed streaks was observed and small particles with $St^+ < 1$ were found to suppress turbulence, while large particles enhanced it, a result observed in their complementary experiments. Li et al. (2001) studied colliding small diameter particles in a vertical channel flow, with the smallest particles having the most significant effect. At increased mass loadings, the turbulence intensities became more anisotropic, with the addition of collisions redistributing the particles more homogenously throughout the wall-normal direction. Zhao et al. (Zhao et al., 2010; Zhao et al., 2013) observed turbulent drag reduction for inertial particles at a range of Stokes numbers based on the shear timescale varying between 1 and 50, with the higher Stokes number particles having the most substantial effect. Turbulence intensities in the streamwise direction were enhanced whereas that in the other two coordinate directions were dampened. Lee and Lee (2015) performed a similar study, with small Stokes number particles increasing the fluid velocity fluctuations and large Stokes number particles dampening them. In this study, all three coordinate directions were affected in the same manner by the presence of particles, however, the particle size and mass loading was fixed and the Stokes numbers were obtained by varying the particle-fluid density ratio.

More recently, Monchaux and Dejoan (2017) studied heavy particles falling through homogenous turbulence, with good agreement being obtained when compared to the experimental work of Aliseda et al. (2002) local fluid quantities were altered by the presence of particles, even at low particle loadings. Dizaji and Marshall (2017) studied the effect of particle-particle agglomeration on turbulence modulation using an adhesive discrete-element method to simulate formation of clusters. It was observed that the agglomeration had little influence on the attenuation of turbulence although two-way coupled computations generated larger agglomerates than the one-way coupled counterpart, with fluid motion inside the particle structures correlating with the agglomerate velocity. Kasbaoui et al. (2019) studied the modification of sheared turbulence by particles, linking the ideas of rapid distortion theory to two-way coupled flows and providing an explanation for the shear-induced production of turbulence.

The focus in recent years has shifted to understanding the effects of gravitation on two-way coupled flows, with many questions surrounding the emergent behaviour based on different mass-loadings left unanswered. The present study addresses these questions by investigating how particles with different density ratios affect the modulation of turbulence, with a focus on the topology of the coherent turbulent structures present in these flows. The PSIC technique is implemented to achieve particle-fluid coupling and a hard sphere perfectly elastic collision detection and resolution algorithm is used to introduce four-way coupling. This study considers three distinct Stokes numbers ($St^+ = 0.1, 50, 92$), obtained by modifying the density ratio, with a fixed particle diameter relative to the channel half-height, $d_P^* = 0.005$.

II. METHODOLOGY

A. Channel flow simulation

Direct numerical simulation is employed using the open-source code, Nek5000 (Fischer et al., 2008) which uses a high-order spectral element method to simulate the fluid phase to a high degree of accuracy wherein all relevant turbulence length and timescales are fully resolved. The governing equations for the continuous phase are the dimensionless incompressible continuity and Navier-Stokes equations, given by:

$$\boldsymbol{\nabla} \cdot \boldsymbol{u}^* = 0, \tag{1}$$

$$\frac{D\boldsymbol{u}^*}{Dt^*} = -\boldsymbol{\nabla} p^* + \frac{1}{Re_B}\nabla^2 \boldsymbol{u}^* + \boldsymbol{f}_{PG}^* + \boldsymbol{f}_{2W}^*, \tag{2}$$

where $\boldsymbol{u}^*$ is the fluid velocity vector, p^* is the fluid pressure, Re_B is the bulk Reynolds number defined as $Re_B = U_B\delta/\nu_F$, and ν_F is the fluid kinematic viscosity. These equations are non-dimensionalised using the channel half-height, δ, the bulk fluid velocity, U_B, and the fluid phase density, ρ_F. From here on, a quantity with an asterisk (*) denotes a variable non-dimensionalised in this manner. The term $\boldsymbol{f}_{PG}^*$ represents the constant pressure gradient, homogeneous forcing term orientated in the streamwise direction, which has magnitude:

$$\frac{\partial p^*}{\partial x^*} = \left(\frac{Re_\tau}{Re_B}\right)^2. \tag{3}$$

Here, $Re_\tau = u_\tau\delta/\nu_F$ represents the shear Reynolds number in the absence of particles, with $u_\tau = \sqrt{\tau_W/\rho_F}$ the shear velocity and τ_W the mean shear stress at the wall boundary. In this sense, the flow is driven by a constant force which is unrelated to the presence of particles within the flow. For all simulations considered within this study, the shear Reynolds number was set to be constant at $Re_\tau = 180$, due to this particular system having been extensively simulated, validated and understood for the unladen case. The corresponding bulk Reynolds number is $Re_B = 2800$. The term $\boldsymbol{f}_{2W}^*$ represents the point-source two-way coupling momentum exchange term between the particles and the surrounding fluid. The technique ignores the physical displacement of the local fluid surrounding the particle, but since the particle diameter considered is smaller than the grid spacing, it is viable to use the PSIC method of obtaining two-way coupling so long as the volume fraction remains sufficiently low. By satisfying these conditions, the short-range perturbations are dissipated by the fluid viscosity and so the undisturbed cell velocities are approximately equivalent to the disturbed cell velocities. Since the focus of this work is on determining the effects of particles on vortical structures, we also compare the particle size to the size of these structures. In all simulations considered, the particle size is less than a third of the Kolmogorov length scale, meaning that for even the smallest turbulence structures, the trajectory through the structure will be resolved, so long as the timestep is sufficiently low. Hence, the spatially and temporally developing feedback field caused by a single particle will be smooth and locally distributed. The equation for the acceleration source term in the Navier-Stokes equations is as follows:

$$\boldsymbol{f}_{2W}^{*i} = -\frac{m_p}{m_F}\sum_{j}^{N_{P,i}} \frac{\partial \boldsymbol{u}_{P_j}^*}{\partial t^*}, \tag{4}$$

where m_p is the mass of each particle, m_F is mass of the fluid within the integration volume, and j is an index which iterates over the number of particles contained within the corresponding cell, $N_{P,i}$. The variables within in the summation are related to the Lagrangian particle tracking (LPT) algorithm and will be introduced in Section IIB. Note that this term is a non-dimensional acceleration which is subsequently multiplied by the fluid density in the momentum equation.

The geometry considered in this study is that of a wall-bounded channel flow, which is discretized onto a structured Cartesian grid consisting of $27 \times 18 \times 23$ 7th-order spectral elements, chosen to ensure that the mean spacing of GLL nodes is on the order of the Kolmogorov scale (see Mortimer et al. (2019)). Elements located close to the wall are distributed in the wall-normal (y) direction more densely in order to resolve the small-scale turbulent structures in those regions. Elements in the streamwise (x) and spanwise (z) directions are distributed evenly. A channel flow computational domain schematic is presented in Figure 1 and has dimensions $14\delta \times 2\delta \times 6\delta$. The upper and lower bounds of the wall-normal direction enforce no-slip and impermeability conditions, whereas the other two directions are periodic at either end.

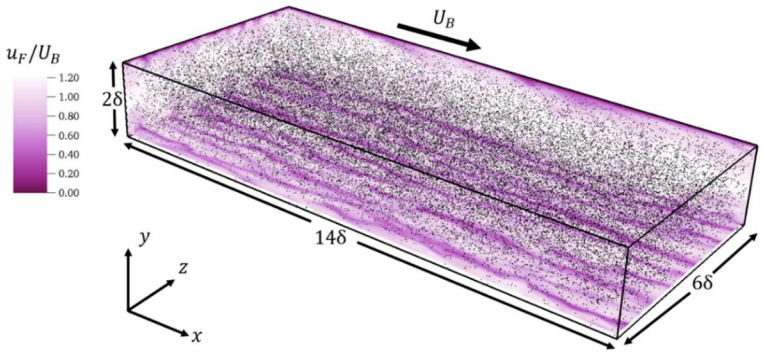

Figure 1: Schematic of the multiphase turbulent channel flow at $Re_\tau = 180$. Colour indicates fluid velocity magnitude non-dimensionalised by the bulk flow velocity, U_B. Black spheres indicate locations of particles.

A constant fluid solver timestep of $\Delta t^* = 0.005$ is used consistently and is below that of the smallest particle response time, and the initial condition uses a laminar profile which contains minor perturbations in the off-streamwise directions in order to encourage the transition to turbulence. An initial unladen simulation was performed until $t^* = 1000$, during which first- and second-order flow statistics were monitored. After they had reached a statistically stationary state, the statistics were resampled between bulk times $500 < t^* \leq 1000$ for validation and analysis purposes.

B. Lagrangian particle tracking

The LPT routine applied in Mortimer et al. (2019) was used to compute the trajectories of solid particles throughout the channel flow. In this approach, it is assumed that each element of the discrete phase is an undeformable, impenetrable point-like sphere, which is on the same scale as or smaller than the Kolmogorov scale in all regions of the flow. After a continuous phase timestep is completed, the LPT spectrally interpolates key fluid observables (instantaneous velocity and deviatoric tensor components) onto the position of each particle in the flow. This information is then used to solve the force-balance equation (Maxey and Riley, 1983; Maxey, 1987; Riley and Patterson Jr, 1974) for

each particle, integrated to update the particle position and velocity over the course of a timestep. In our previous work (Mortimer et al., 2019), it was determined that all hydrodynamic forces (drag, lift, pressure gradient and virtual mass) are relevant across the range of Stokes numbers and density ratios considered in this study. Gravitational and buoyancy forces were excluded since the present study focuses on elucidating the mechanisms by which coherent turbulent structures are altered by the presence of particles, and additional gravity-related behaviour such as settling would introduce complexity to the understanding. The Basset history force has been neglected due to previous work exhibiting very little effect on the particle motion upon its inclusion (Fairweather and Hurn, 2008; Daitche, 2015). With these neglections, the Newtonian equations of motion for each point-sphere are:

$$\frac{\partial \boldsymbol{x}_P^*}{\partial t^*} = \boldsymbol{u}_P^*, \tag{5}$$

$$\frac{\partial \boldsymbol{u}_P^*}{\partial t^*} = \frac{1}{\mathrm{M_{VM}}}\left[\underbrace{\frac{3C_D|\boldsymbol{u}_S^*|}{4d_p^*\rho_P^*}\boldsymbol{u}_S^*}_{Drag} + \underbrace{\frac{3}{4}\frac{C_L}{\rho_P^*}(\boldsymbol{u}_S^* \times \boldsymbol{\omega}_F^*)}_{Lift} + \underbrace{\frac{1}{2\rho_P^*}\frac{D\boldsymbol{u}_F^*}{Dt^*}}_{Virtual\ Mass} + \underbrace{\frac{1}{\rho_P^*}\frac{D\boldsymbol{u}_F^*}{Dt^*}}_{Pressure\ Gradient}\right]. \tag{6}$$

Here, $\boldsymbol{x}_P^*$ is the particle position vector, $\boldsymbol{u}_P^*$ is the particle velocity vector, $\boldsymbol{u}_F^*$ is the spectrally interpolated fluid velocity vector at the position of the particle, $\boldsymbol{u}_S^* = \boldsymbol{u}_F^* - \boldsymbol{u}_P^*$ is the slip velocity between the fluid and the particle, d_P^* is the particle diameter non-dimensionalised by the channel half-height, ρ_P^* is the density ratio between the fluid and the particle and $\boldsymbol{\omega}_F^* = \boldsymbol{\nabla} \times \boldsymbol{u}_F^*$ is the vorticity of the fluid spectrally interpolated at the particle position. $\mathrm{M_{VM}}$ is the virtual mass, and C_D and C_L are the drag and lift coefficients, respectively. Further details surrounding the calculation and origin of these terms are presented in Mortimer et al. (2019). Eqs. (5) and (6) are solved using a fourth order Runge-Kutta scheme, with the integration timestep equal to that used by the continuous phase solver.

Table 1: Particulate phase parameters for multiphase turbulent channel flow simulation at $Re_\tau = 180$.

Parameter	**$St^+ \approx 0.1$**	**$St^+ \approx 50$**	**$St^+ \approx 92$**
Particle diameter, d_P^*	0.005	0.005	0.005
Particle diameter, d_P^+	0.9	0.9	0.9
Number of particles, N_P	300,000	300,000	300,000
Shear Stokes number, St_τ	0.113	49.995	91.845
Bulk Stokes number, St_B	0.01	4.321	7.937
Density ratio, ρ_P^*	2.5	1111	2041
Volume fraction, Θ_P	10^{-4}	10^{-4}	10^{-4}
Particle and fluid timestep, Δt*	0.005	0.005	0.005
Particle and fluid timestep, Δt^+	0.0575	0.0575	0.0575

Particles are initially injected randomly throughout the entirety of the domain, and are reflected elastically upon collision with any of the wall boundaries. Particles leaving through a periodic boundary are reinjected into the other side of the domain at the corresponding position. Importantly, in both of these boundary-interaction mechanisms the distance travelled within the timestep is conserved. For example, when colliding with a wall, extra calculations are performed to ensure the particle reflects off the wall the same distance it travelled virtually 'through' the boundary. Interparticle collisions are not considered in this study since the volume fraction is sufficiently low ($\Theta_P < 10^{-3}$). In this regime, collisions occur infrequently enough such that the turbulence is unaffected by the redistribution of slip velocities in a collision event.

It is useful to characterize spherical particles in solid-fluid multiphase turbulent flows by their Stokes number. This measures the particle response timescale to a suitable system-specific fluid timescale, such as the bulk timescale, $\tau_{FB} = \delta/U_B$, or the shear/viscous timescale, $\tau_{F\nu} = \nu_F/u_\tau^2$. Hence, the Stokes numbers for a given particle in this study are given by $St_B = \tau_P/\tau_{FB}$ for the bulk scale and $St^+ = \tau_P^+ = \tau_P/\tau_{F\nu}$ for the shear or viscous scale. Here, τ_P is the relaxation time of the particle, given by $\tau_P = \rho_P^* d_P^2/18\nu_F$. In the present work we fix the particle diameter and obtain a desired Stokes number by varying the density ratio between the particle and the fluid. Furthermore, Stokes numbers across a broad range are considered, ranging from $St^+ \approx 0.1$, representative of glass particles in water, to $St^+ \approx 92$, representative of glass particles in air. The number of particles was chosen to ensure that the volume fraction ($\Theta_P = 10^{-4}$) is within the regime suggested by Elghobashi (2007) within which two-way coupling effects are important. The choice of parameters here have been carefully selected to represent typical values in a $\delta = 0.02m$ channel flow, which is a common comparative system for flows such as these. For instance, $d_P^* = 0.005$ is equivalent to considering a $100\mu m$ particle, which are common in many processing industries. The variation of diameter has been studied extensively in recent years (Ferrante and Elghobashi, 2003; Vreman et al., 2009) with d_P/η_K being a significant quantity to determine coupling behaviour. The Reynolds number was chosen due to its extensive consideration in previous studies as well as because of the demonstrated scaling of particle migration and interaction mechanisms with this property (Bernardini, 2014). Parameters for each simulation considered in this study are presented in Table 1.

III. RESULTS AND DISCUSSION

A. Validation of the two-way coupling mechanism

Before presenting the results of the simulations listed in the methodology, an initial validation simulation was performed against a previous DNS study performed by Lee and Lee (2015) in order to validate the implementation of the method.

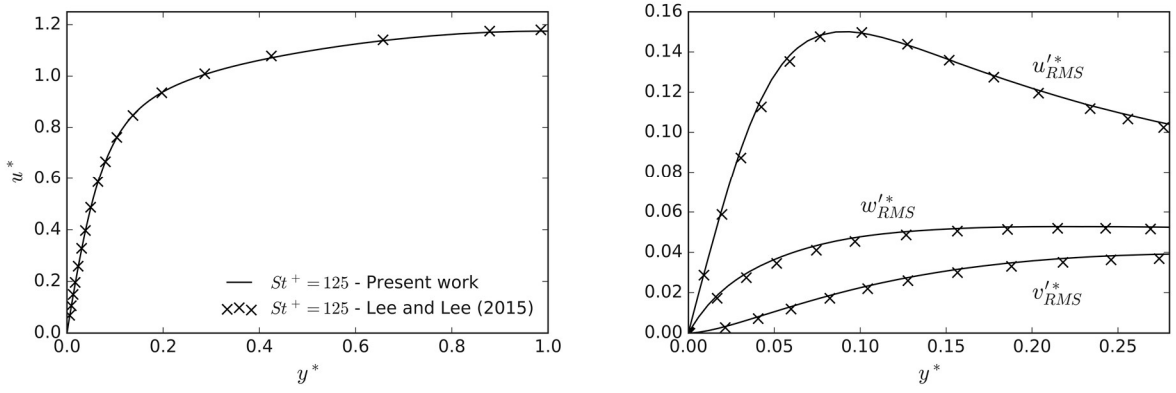

Figure 2: Validation of two-way coupling mechanism with Lee and Lee (2015). Comparison of fluid mean streamwise velocity (left) and root mean square of velocity fluctuations (right) sampled at $t^+ = 500$ after particle injection.

Parameters such as volume fraction, channel dimensions, integration timestep, sampling time and Reynolds number were identical between this validation and the compared study. Here, we demonstrate the results obtained from the largest Stokes number particle species considered by the authors, $St^+ = 125$. The first- and second-order velocity statistics for the two-way coupled particle-laden validation flows

are compared in Figure 2. Excellent agreement between the previously carried out DNS and the present study is obtained which is indicative of the reliability and reproducibility of the point-particle coupling method, even across different continuous phase solvers.

B. Temporal evolution of turbulence modulation

Upon injection of a suitably large mass fraction of particles, a turbulent multiphase flow will undergo a transition wherein the inherent structure of the turbulence will be altered due to the presence of the solid phase. During this time, other mechanisms observed even in one-way coupled flows, such as turbophoresis and preferential concentration, will also begin to take place which has consequences for the magnitude and nature of the two-way coupling effects. This means that turbulence modulation is time-sensitive, and likely does not ever reach a truly statistically steady state. Furthermore, the timescales during which the modulation effects occur will depend strongly on the Stokes number of the injected particle species, since turbophoretic drift is greatest when the particle response time is around 2-3 times greater than the bulk timescale, based on previous studies (Picciotto et al., 2005; Kuerten and Vreman, 2005; Sardina et al., 2012).

In this study, we first consider the time evolution of the first- and second- order turbulence statistics gathered over equal time segments with length $t^* = 20$ (over a period of $0 \leq t^* \leq 100$) in order to better understand this transitional phase. Note that time, t^*, is now measured from the moment of injection of particles into the statistically stationary unladen turbulent channel flow. We discuss here the case which exhibited the most time-sensitive results, and these are presented in Figure 3. The evolution of the mean streamwise velocity due to the presence of particles is illustrated in the upper left plot. Over the course of the simulation, this quantity increases with the greatest effects exhibited at the channel centre. The overall trend of an increasing mean fluid velocity profile with time has been previously observed in the literature for spherical particles (Li et al., 2001; Zhao et al., 2010) as well as for the addition of polymer additives (Lumley, 1973). Clearly by $t^* = 100$ the modulation is slowing, with the greatest effects taking place over this timeframe. Similar observations were made for the $St^+ = 50$ particles, however the initial transitory period was shorter and the reduction of streamwise rms velocity fluctuations was less pronounced. Samples were also taken at $t^* = 120$ for all cases which exhibited very insignificant change from those obtained at $t^* = 100$. The system appears to demonstrate two timescales across which the turbulence modulation dynamics occur. The first is the initial timescale associated with the initial reaction of the flow to the injection of the particulate phase. The second is a much longer timescale wherein turbophoresis slowly redistributes the particles towards the wall-region.

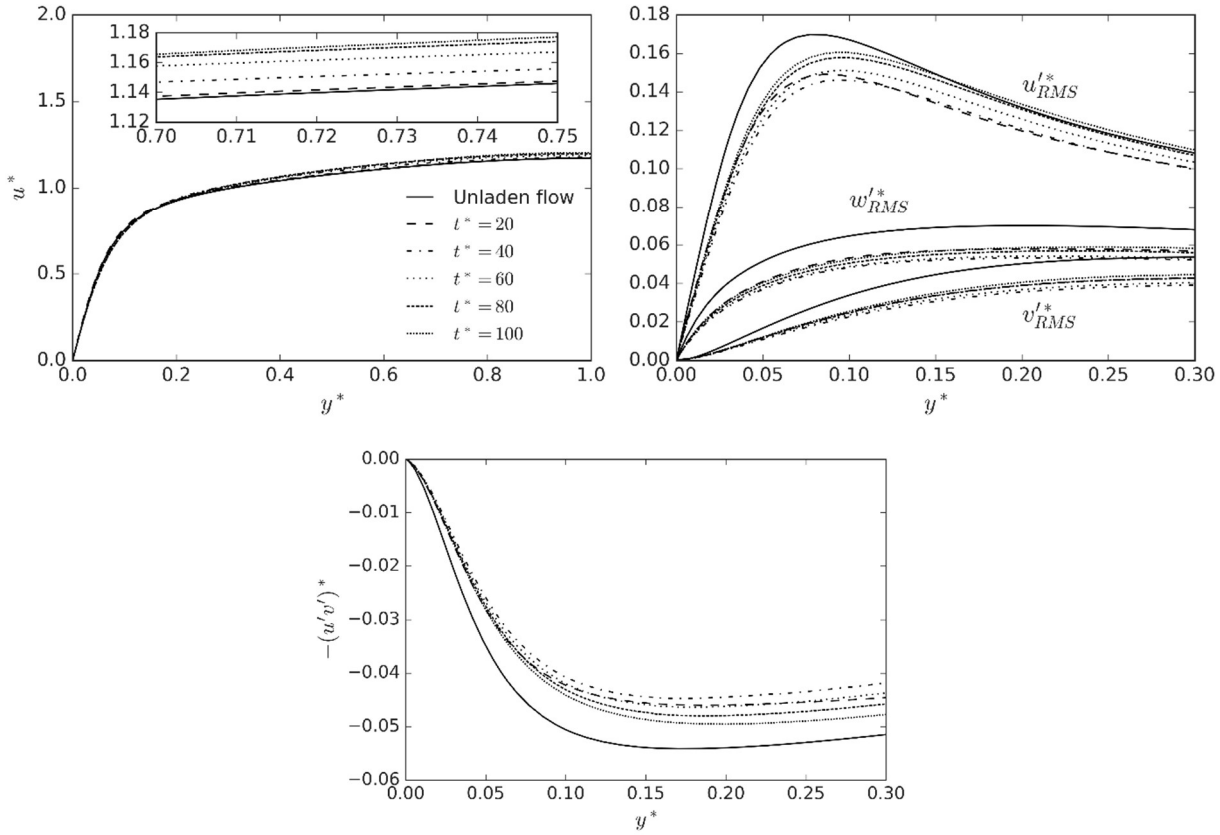

Figure 3: Time evolution of fluid mean streamwise velocity (upper left), root mean square of velocity fluctuations (upper right) and shear stress (lower) for two-way coupled particle-laden turbulent channel flow at $St^+ = 92$.

The upper right plot shows how the presence of the particles affects each component of the rms velocity fluctuations close to the wall, at $y^* < 0.3$. Remarkably, all three components are reduced and reach their minima at around $t^* = 40$ before the turbulence begins to increase again. Eventually, the streamwise component is increased compared to that of the unladen flow in the centre of the channel, with the peak in the profile also shifted towards the centre. In the wall region, however, and everywhere for the off-streamwise components, the rms velocity fluctuations are dampened. Similar observations can be made for the shear stress component in the lower plot which is initially greatly dampened, before again increasing (in magnitude). This behaviour is in agreement with previous work (Lee and Lee, 2015; Zhao et al., 2010; De Marchis and Milici, 2016), but here we show that the measured magnitude of the turbulence modulation is highly sensitive with time, particularly within the first 100 bulk time units. Since the simulations performed are computationally costly, and thus limited to relatively low simulation times, this is something of importance that must be considered in analysing such flows.

C. Effect of Stokes number on turbulence modulation and structure

The effect of particle Stokes number on the first- and second- order flow field statistics, beyond $t^* = 100$, is presented in Figure 4 to Figure 6. The mean streamwise velocity profile (Figure 4) is the least affected, particularly so close to the wall. Recalculation of the shear Reynolds number due to modification of the wall shear stress yields negligible variation. The heaviest particles increase u^* in the bulk region ($y^* > 0.2$) and reduce it in the buffer layer. For the lightest particles at $St^+ = 0.1$, there is very little deviation in mean streamwise velocity from that of the unladen flow. The rms velocity fluctuations (Figure 4) show a greater response to the presence of the particles. Specifically, inertial

particles with $St^+ \gg 1$ attenuate the off-streamwise components everywhere in the flow, and the streamwise component in the near-wall region. The $St^+ = 0.1$ particles enhance the streamwise component of turbulence slightly, particularly so close to the wall and near the channel centre. Unlike previous findings (Lee and Lee, 2015), suppression of turbulence is not most effective at mid-range Stokes numbers ($St^+ \approx 25$), and continues to scale with Stokes number far beyond this range. However, the authors chose to fix mass fraction, whereas in the present study we isolate the effects of modifying this quantity. This observation suggests that the extent of modulation scales more with the mass fraction of particles than it does with a combination of density ratio and diameter. The dominating factor leading to turbulence suppression in the present simulations is therefore particle inertia, rather than turbophoresis or preferential concentration.

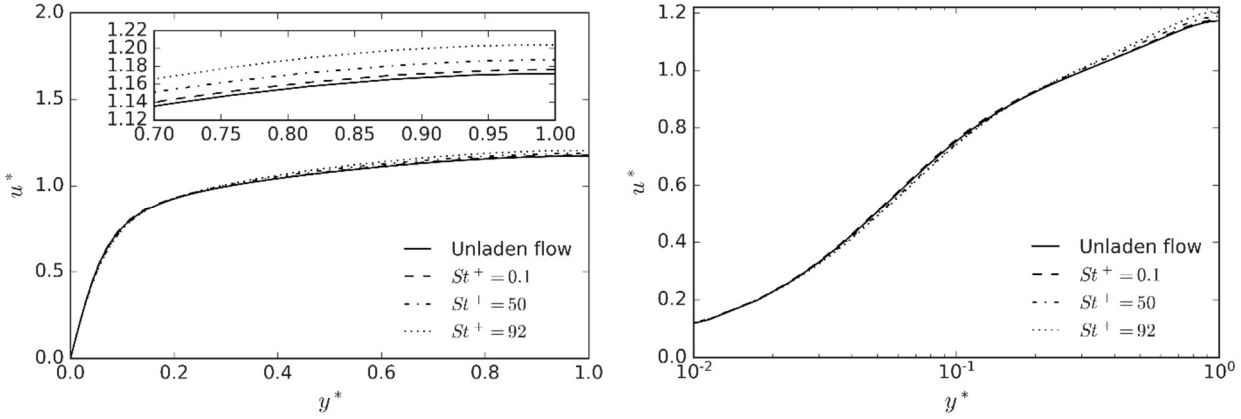

Figure 4: Mean streamwise fluid velocities normalized by the bulk velocity, U_B, for two-way coupled particle-laden channel flow. Right plot is on a log scale.

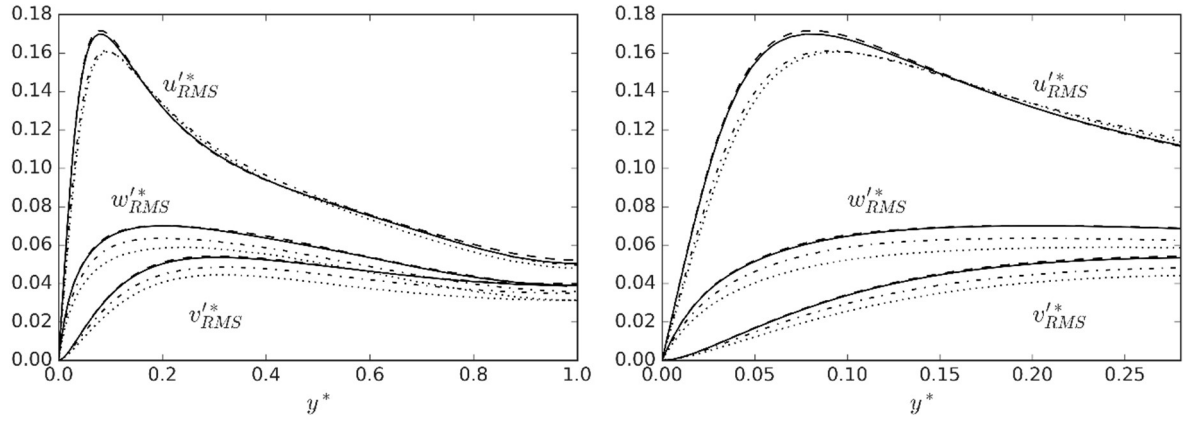

Figure 5: Root mean square of fluid velocity fluctuations normalized by the bulk velocity, U_B, for two-way coupled particle-laden channel flow. Right plot illustrates near-wall region behaviour. Legend for both plots is same as Figure 4.

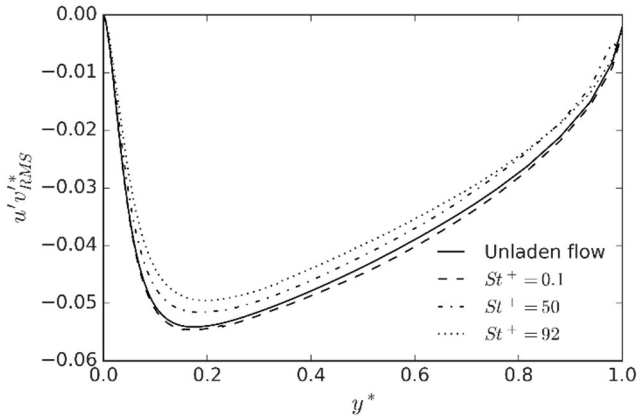

Figure 6: Fluid shear stress normalized by the bulk velocity, U_B, for two-way coupled particle-laden channel flow.

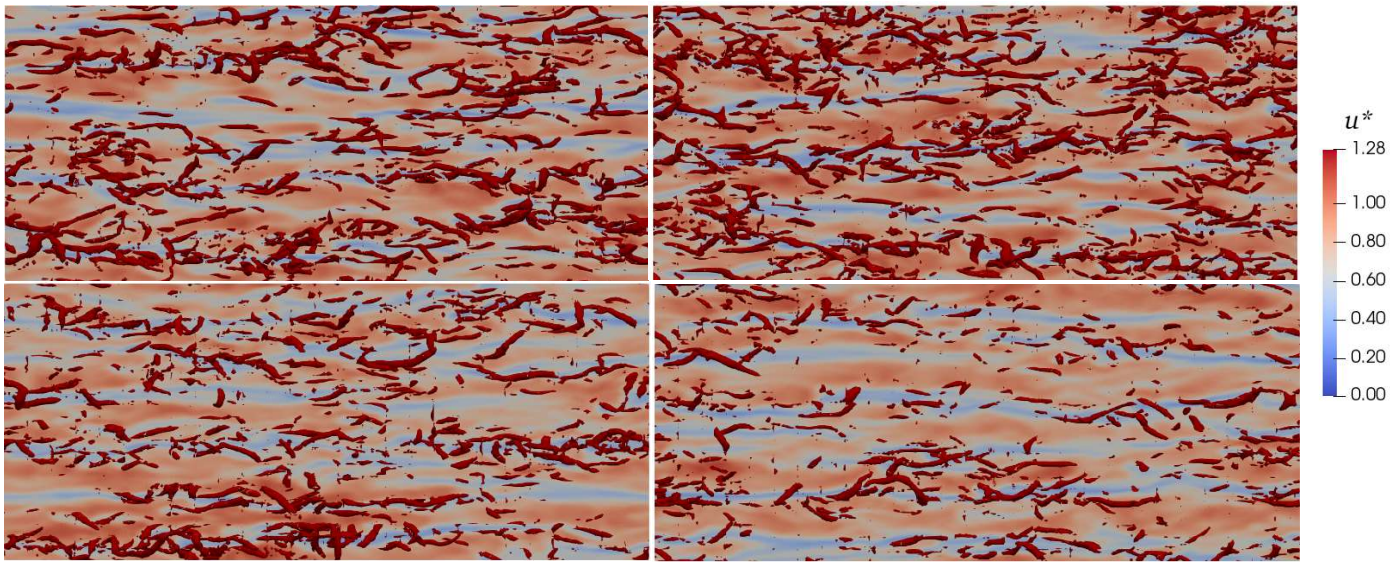

Figure 7: Q-criterion isosurfaces (in red) overlaying instantaneous velocity magnitude at $y^* = 0.1$ for unladen flow (upper left), $St^+ = 0.1$ (upper right), $St^+ = 50$ (lower left) and $St^+ = 92$ (lower right).

There are a variety of methods used to classify coherent turbulent flow structures. A commonly employed subset of these are those based on the velocity gradient tensor, $D_{ij} = \frac{\partial u_i}{\partial x_j}$. This tensor is often decomposed into its symmetric (rate-of-strain) and antisymmetric (vorticity) tensor components such that $D_{ij} = S_{ij} + \Omega_{ij}$, with $S_{ij} = \frac{1}{2}\left(\frac{\partial u_i}{\partial x_j} + \frac{\partial u_j}{\partial x_i}\right)$ and $\Omega_{ij} = \frac{1}{2}\left(\frac{\partial u_i}{\partial x_j} - \frac{\partial u_j}{\partial x_i}\right)$. The Q-criterion (Hunt et al., 1988) refers to conditions applied to the second invariant, Q, of the velocity gradient tensor, where $Q = \frac{1}{2}(\Omega^2 - S^2)$. This condition is such that if $Q > 0$ (i.e. the vorticity is greater than the shear strain rate) is satisfied in a particular fluid cell then the fluid element contains part of a vortex.

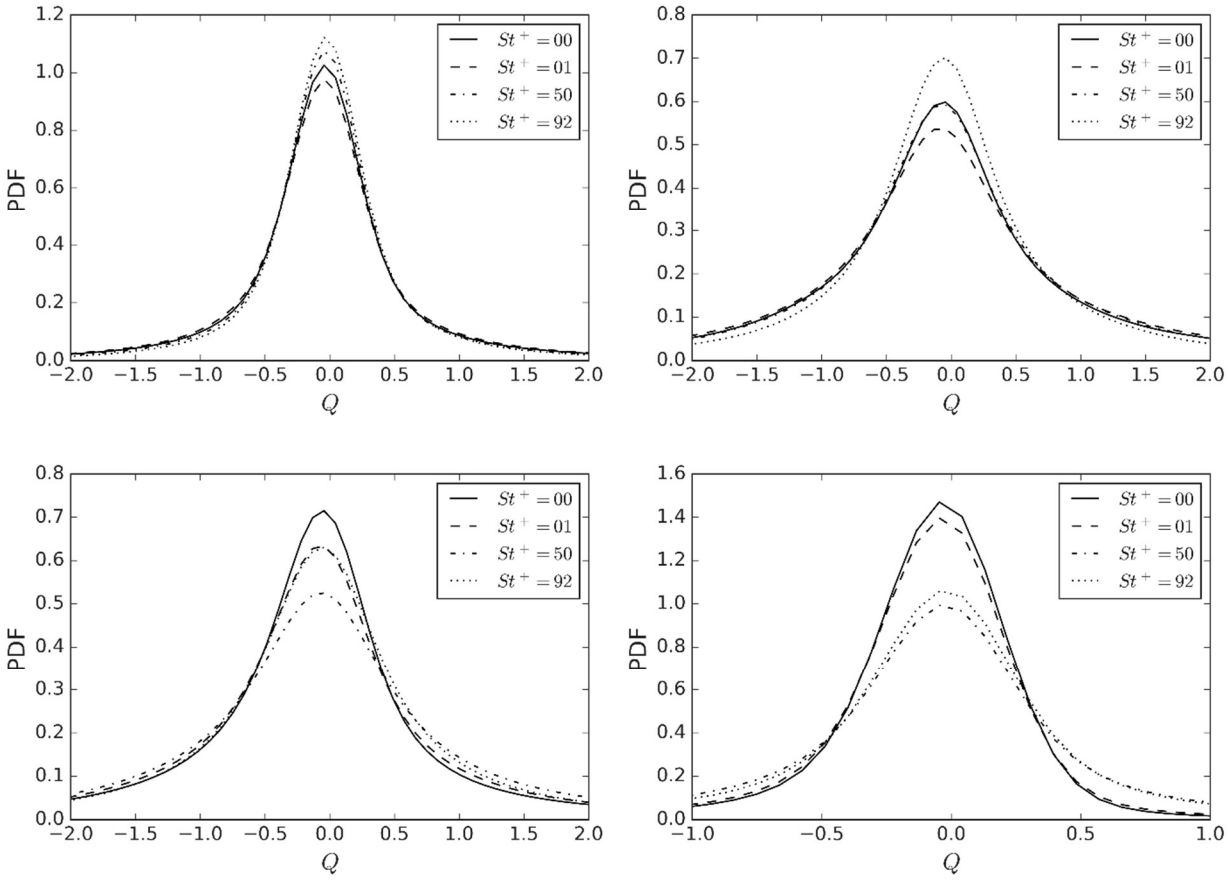

Figure 8: Probability density functions of second fluid velocity deviatoric tensor invariant, Q, in wall-normal channel regions. Upper left: bulk flow, upper right: log-law, lower left: buffer layer, lower right: viscous sublayer.

In

Figure 7 we illustrate the effect of particles on the instantaneous flow field isosurfaces of Q-criterion on $x-z$ planes close to the channel wall ($y^* = 0.1$) in order to determine how turbulence modulation affects the structure and frequency of vortical regions. Comparing the upper-right plot ($St^+ = 0.1$) to the upper-left plot (unladen flow), we observe that the frequency of coherent turbulent structures increases. For the lower two plots, $St^+ = 50$ and $St^+ = 92$, the presence of particles reduces the number of vortical regions, which is most prevalent for particles with the highest density ratio. These findings are consistent with those presented in Figure 5 where low-density ratio particles slightly increase the rms velocity fluctuations close to the wall, with the opposite trend true for inertial particles.

In Figure 8, the probability density function (PDF) for the distribution of Q is plotted for each Stokes number particles as well as for each classical wall-normal region of the turbulent channel flow. Note that these plots only display the peak region of the curve, but the tails of the distribution extend on either side. These PDFs were sampled using the fluid velocity from all unique GLL points within the discretized domain at $t^* = 100$, with the sample size varying based on channel flow wall-normal region but ranging between ~300,000 and ~4,000,000. The wall-normal region definitions are presented in Table 2. Starting with the upper left plot, which is the bulk region, the addition of particles shows the least effect, with only a slight widening of the peak for the tracer-like particles and narrowing of the peak for the inertial particles, which scales with Stokes number. In this case, a narrower peak implies that the rate of strain becomes closer to the vorticity and in all cases

the peak remains to the left of the $Q = 0$ line, with no obvious increases in the number of Q-criterion satisfying regions. As the wall is approached, the upper right plot indicates more remarkable behaviour in the log-law region. We observe a narrowing of the peak in the case of inertial particles indicating lower-strength vortices, and the $St^+ = 0.1$ particle species produce a widening effect. The $St^+ = 50$ particles preserve the distribution of Q within this region. In the case of the buffer layer (lower left), the presence of particles widens the distribution of Q in all three cases, with the most inertial particles having the greatest effect, and the two other species exhibiting similar qualitative behaviour. Finally, the lower right plot represents the effects in the viscous sublayer, which shows a similar peak width increase, with the inertial particles showing the greatest effect.

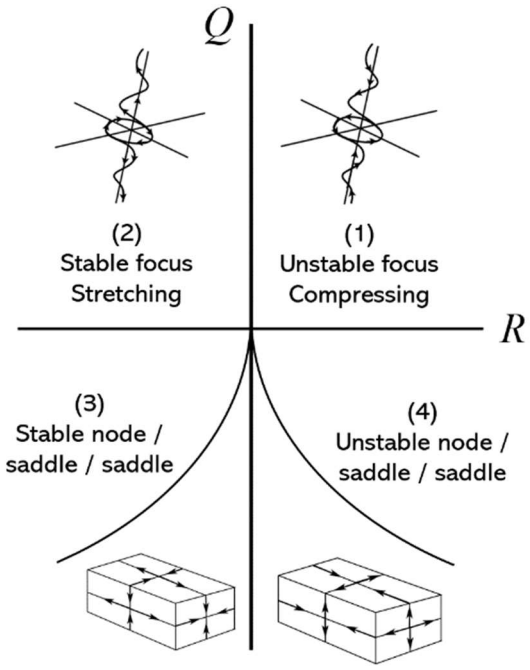

Figure 9: Q and R tensor invariants for incompressible flow turbulent structure topology classification. Solid curved lines represent $D = \left(\frac{27}{4}\right)R^2 + Q^3 = 0$. Region terminology is after (Chong et al., 1990).

Clearly, from these plots alone it is difficult to discern the full effect on the structure of turbulence. In order to do so, we adopt the classification scheme of (Blackburn et al., 1996), in which each fluid field point is categorized as one of four turbulent structure topology definitions. These are unstable focus / compressing, stable focus / stretching, stable node / saddle / saddle and unstable node / saddle / saddle which are illustrated in Figure 9. Here, $R = -tr(D_{ij})$ is the third invariant of the velocity deviatoric tensor.

Table 2: Turbulent channel flow at $Re_\tau = 180$ wall-normal distance region classification.

Region	Distance from wall (*) (begins)	Distance from wall (*) (ends)
Bulk flow	0.200	1.000
Log-law	0.166	0.200
Buffer layer	0.027	0.166
Viscous sublayer	0.000	0.027

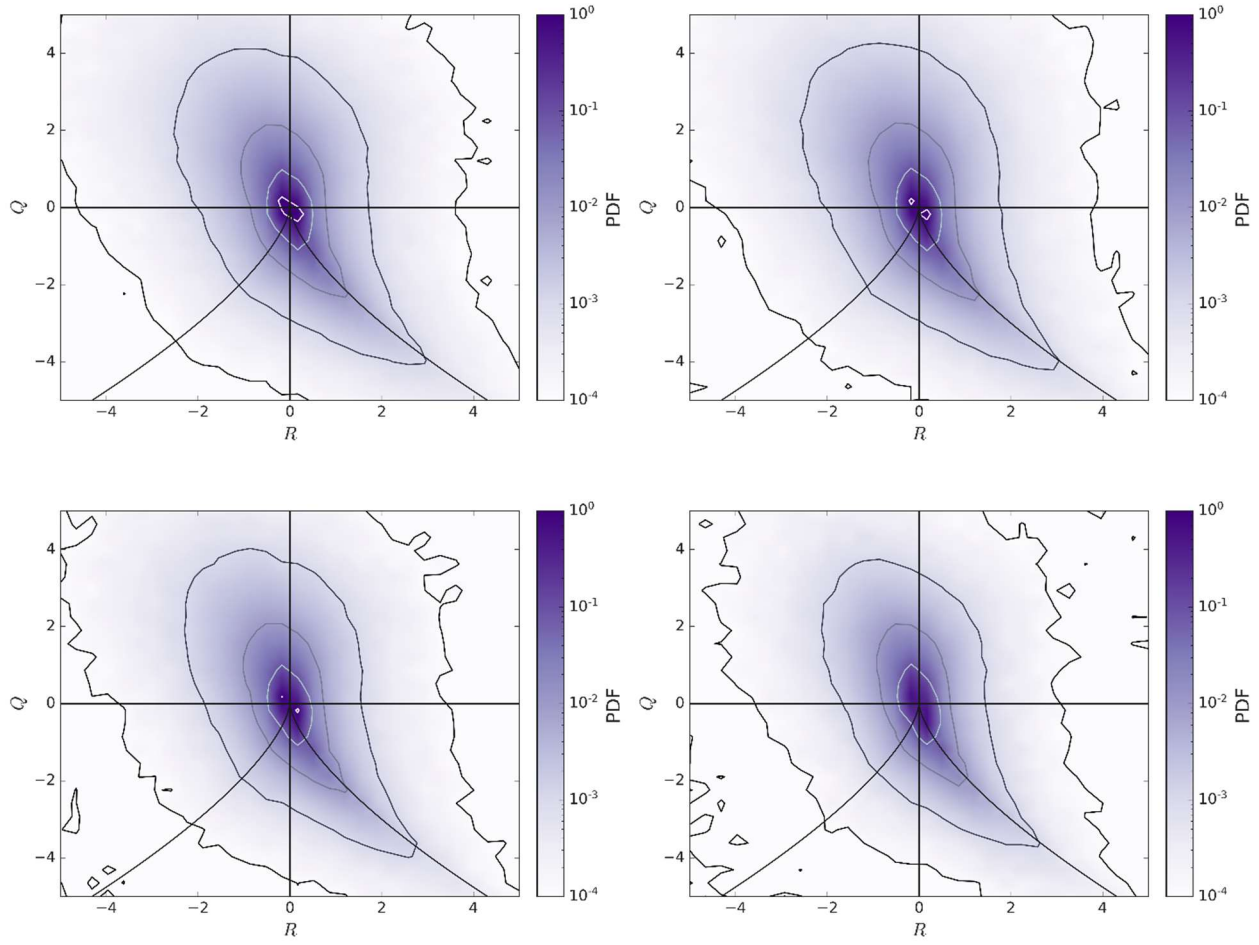

Figure 10: PDFs of invariants of the velocity gradient tensor, Q and R, sampled at fluid nodes and particle positions in the bulk region. Upper left: unladen flow, upper right: $St^{+} = 0.1$, lower left: $St^{+} = 50$, lower right: $St^{+} = 92$.

To perform this analysis, Q and R on fluid grid points were sampled homogeneously for each particle species as well as for the unladen flow in all four channel flow regions. The effect of particles on the combined PDFs of Q and R in the bulk region is presented in Figure 10. The distributions are comparable in all four cases, indicating very little influence of coupling on the turbulent structures which reside close to the centre of the channel flow. Previous studies (Mortimer et al., 2019; Rouson and Eaton, 2001) indicate that particles within this region exhibit very little preferential concentration when compared to other regions of the flow, and slip velocities are the lowest within this region, such that the coupling force and momentum exchange between the two phases will be limited. This is in line with the findings of Figure 8, but we further see that the stability of the area of the fluid fixed points is barely altered. In the bulk flow region, the Kolmogorov length scale is largest, and so the size of turbulence structures in the centre of the channel flow tend to be much bigger. This entails that the coupling strength necessary to alter these structures be greater. Low density-ratio particles possess low slip velocities in this region and hence momentum exchange is limited. For more inertial particles (which may have increased slip velocities), turbophoresis lowers the concentration in this region over time. The combination of these two effects limits the alteration of structures within this region.

The same PDFs are displayed in Figure 11 and Figure 12, this time for the log-law region and the buffer layer, respectively. Both sets of plots show similar behaviour upon the addition of particles and so will be considered together. Comparing firstly the unladen flow (upper

left) with that laden with the two inertial particle species (lower), we observe a general narrowing of the distribution in the R direction, indicating that the frequency of vortical structures is reduced, and that although from Figure 8 we observed similar distributions in Q, the third invariant R is clearly reduced. This means that the stable focus / stretching and unstable focus / compressing type structures are reduced compared to those which reside below the $D = 0$ line (the node / saddle / saddle type fixed points). The tracer-like particles exhibit very little discernible effect in these regions, although we know from Figure 8 that the distribution of Q is widened in both cases.

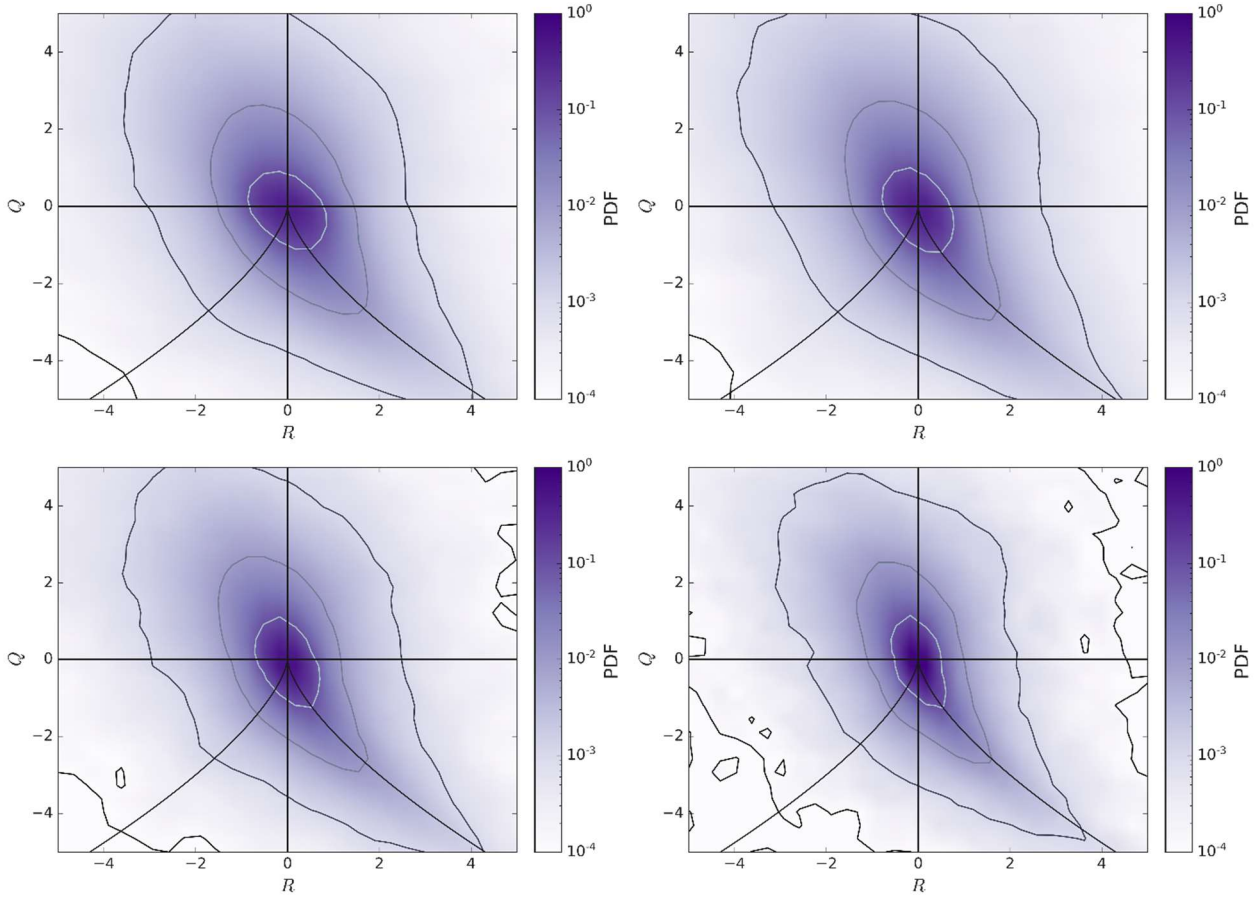

Figure 11: PDFs of invariants of the velocity gradient tensor, Q and R, sampled at fluid nodes and particle positions in the log-law region. Upper left: unladen flow, upper right: $St^+ = 0.1$, lower left: $St^+ = 50$, lower right: $St^+ = 92$.

The most interesting modifications to the turbulent structures due to the presence of particles occur in the viscous sublayer. Comparing the plots in Figure 13, an initial observation is that in all three particle cases, the addition of particles increases the occurrence of vortical structures in this region. In particular, the tracer-like particles increase the frequency of vortical regions with increased R (upper right), whereas both inertial particle sets increase the frequency of vortices in this region with increased Q. For $St^+ = 50$ the particles increase the frequency of stable focus / stretching regions more so than the unstable focus / compressing regions. By $St^+ = 92$ these vortex-stretching regions are less frequent, and the distribution begins to narrow again in R. From a topological perspective, the stretching in Q corresponds to the local flow becoming more two-dimensional. At these increased Stokes numbers, the turbulence damping due to particle-fluid interaction which occurs in this region may also be responsible for the attenuation in the above layers, where the concentration is lower but we still see significant reduction. These plots indicate that the PSIC method is capable of altering nature of the velocity gradient tensor and hence the

structure of turbulence in the near-wall regions. Since the particles considered in this study are smaller than both the GLL spacing and the Kolmogorov length scale, the force distribution over even the smallest eddies will be resolved.

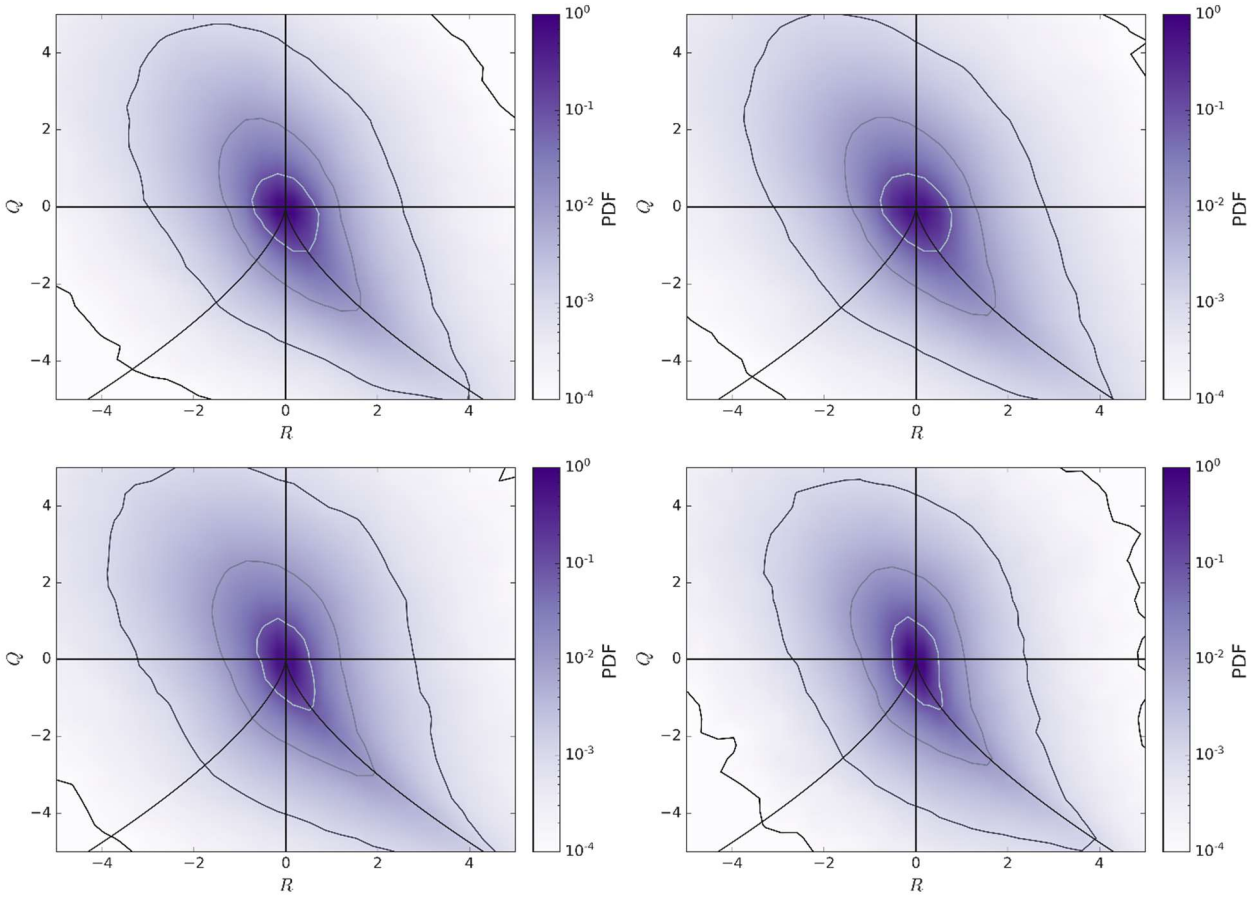

Figure 12: PDFs of invariants of the velocity gradient tensor, Q and R, sampled at fluid nodes and particle positions in the buffer layer. Upper left: unladen flow, upper right: $St^{+} = 0.1$, lower left: $St^{+} = 50$, lower right: $St^{+} = 92$.

C. Effect of Stokes number on particle dispersive and interaction behaviour

In the previous subsection we observed that the presence of particles modifies the inherent structure of turbulence most significantly in three wall-normal regions of the channel flow, although observation of simple attenuation or enhancement of the second-order fluid velocity statistics does not tell the full story. The mechanisms by which vortical regions are modified by particles have been studied in isotropic turbulence (Ferrante and Elghobashi, 2003) based on particle diameter, but mechanisms based on particle inertia as well as for shear flows, such as in channels, are not yet fully understood. In this section, the dispersive and interaction behaviour of each particle species will be considered and related back to the observations made in the previous subsection surrounding the modification of coherent turbulent structures.

In wall-bounded flows, it is known that inertial particles will interact with quasi-streamwise vortices close to the solid boundaries and preferentially accumulate within the near-wall regions (Brooke et al., 1992). We determine the extent of this for the present flow in Figure 14 which illustrates the concentration profiles for each species of particle sampled at $t^{*} = 100$. The tracer-like particles by this time still exhibit a relatively homogeneous concentration profile since the degree of turbophoresis is very weak as the particles' inertia is low. As the Stokes number approaches closer to the critical point at which turbophoresis is maximized, i.e. $St^{+} \approx 30$ (Eaton and Fessler, 1994; Winkler

et al., 2004; Rouson and Eaton, 2001), the concentration profile peaks at the wall. For the most inertial particles, this concentration peak is reduced. Note that there exists a secondary peak at the channel centre for the inertial particles, since this is also a minima of the mean turbulence kinetic energy.

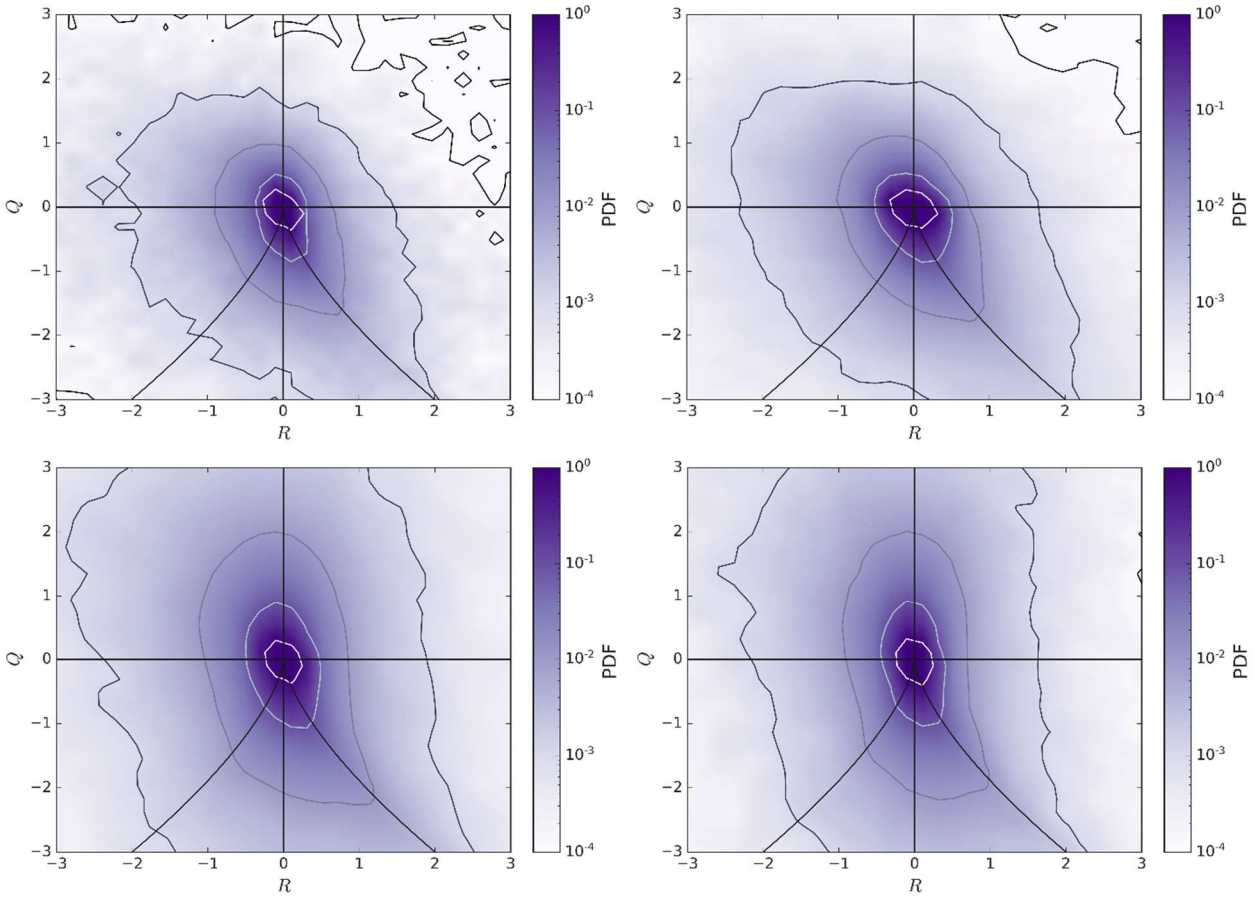

Figure 13: PDFs of invariants of the velocity gradient tensor, Q and R, sampled at fluid nodes and particle positions in the viscous sublayer. Upper left: unladen flow, upper right: $St^+ = 0.1$, lower left: $St^+ = 50$, lower right: $St^+ = 92$.

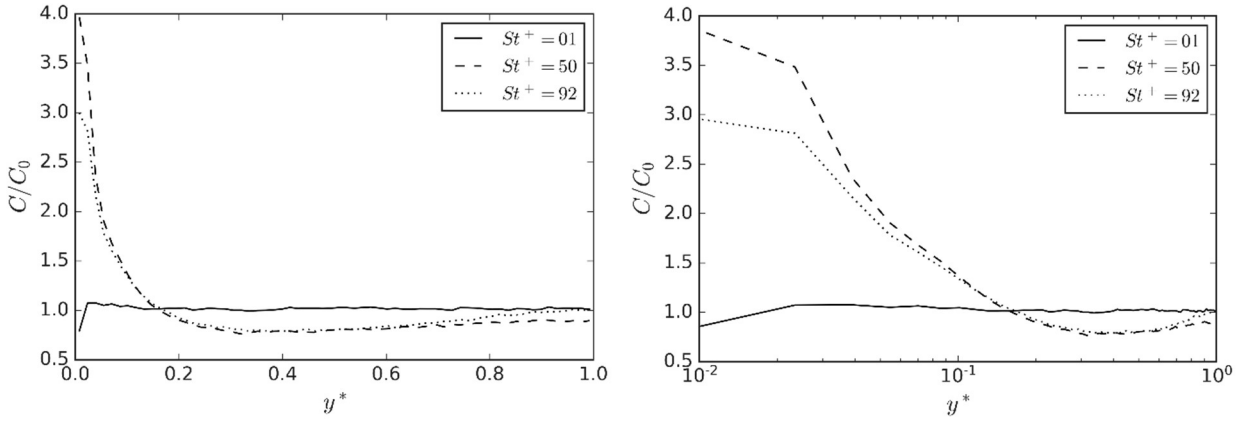

Figure 14: Effect of Stokes number on particle concentration profiles relative to the initial injected concentration sampled at $t^* = 100$. Right graph is plotted on a log scale.

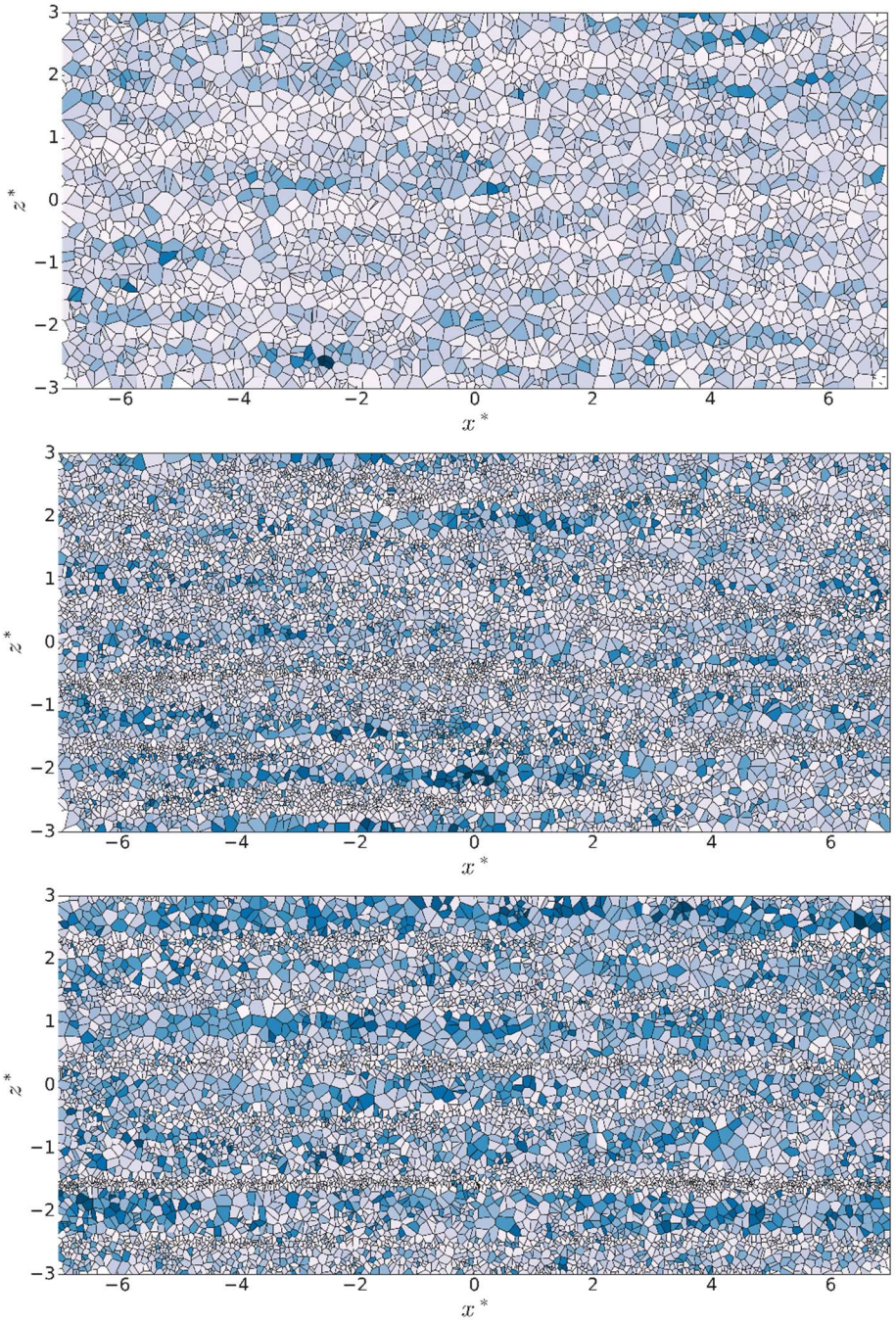

Figure 15: Voronoi analysis of particle positions in the viscous sublayer. Size of cell is inversely proportional to local concentration, colour scale represents particle streamwise velocity (dark colours represent high velocities). Upper: $St^+ = 0.1$, centre: $St^+ = 50$, lower: $St^+ = 92$.

To determine the distribution of particles in the near-wall region, and to further identify the variation of the nature of turbulence structures close to the wall, a Voronoi analysis has been performed on particle (x, z) coordinates within in the viscous sublayer. This is presented in Figure 15, with the colour representing the streamwise velocity magnitude. In line with Figure 14, the $St^+ = 0.1$ particles exhibit the lowest concentration, indicated by the comparatively large cells. Furthermore, the streamwise velocity of these particles is low, showing very little indication of clustering or congregation in low speed streaks. As the Stokes number is increased to $St^+ = 50$, the particle concentration is much greater. Here we observe, however, that the regions of highest particle density indicate particles moving with very low

speeds, whereas the low density regions contain particles with high streamwise velocities. The same behaviour is observed at $St^+ = 92$, although the regions of low concentration are larger, implying an overall lower concentration than for the midrange particle species, in agreement with Figure 14.

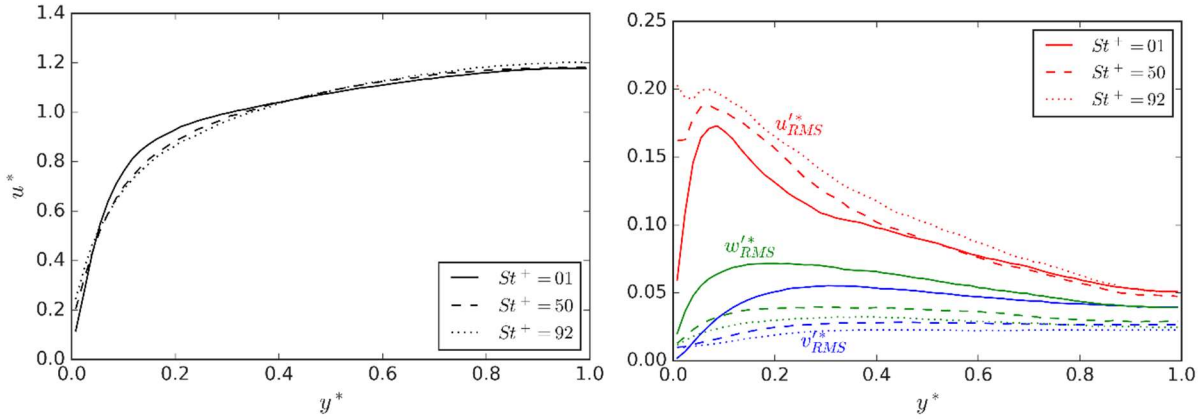

Figure 16: Mean particle streamwise velocity (left) and root mean square of particle velocity fluctuations (right) for two-way coupled particle-laden channel flow at $Re_\tau = 180$. Red: u'^*_{rms}, blue: v'^*_{rms}, green: w'^*_{rms}.

The first- and second-order particle velocity statistics are presented for each Stokes number in Figure 16. From the left plot (mean streamwise velocity) we observe three regions of interest. Between the wall boundary and extending into the log-law region, the particle mean streamwise velocity increases with Stokes number, likely as a result of particles entering these regions through sweeps with retained increased speeds from the outer layer (Mortimer et al., 2019). As a result, particle mean streamwise velocities are reduced in the regions where turbophoresis migrates particles towards the wall, as particles with high velocities preferentially travel towards the near-wall regions and accumulate in low speed streaks (Picciotto et al., 2005). In the core of the channel, the particle streamwise velocity once again correlates with Stokes number. In this region, even the most inertial particles have enough time to attain the fluid velocity and exceed it, likely due to the drag reduction mechanism providing the more dense particles a means to overtake the mean speed of the unladen flow. The rms particle velocity fluctuations also indicate similar behaviour. The streamwise profile exhibits comparable behaviour to that observed in one-way coupled flows at increased particle inertias (Portela et al., 2002; van Wachem et al., 2015; Mortimer et al., 2019), wherein the streamwise component increases in the viscous sublayer. In general, the rms velocity fluctuations are increased in the streamwise direction and suppressed in the off-stream directions, this effect scaling with particle density ratio. These results have consequences for the coupling term since the dominant force in all these simulations is drag which is directly proportional to the magnitude and direction of the particle slip velocity. If the particle velocities fluctuate more anisotropically compared to those of the fluid, the coupling term will be biased towards streamwise orientated forcing, the extent of which is based on the particle density ratio or Stokes number.

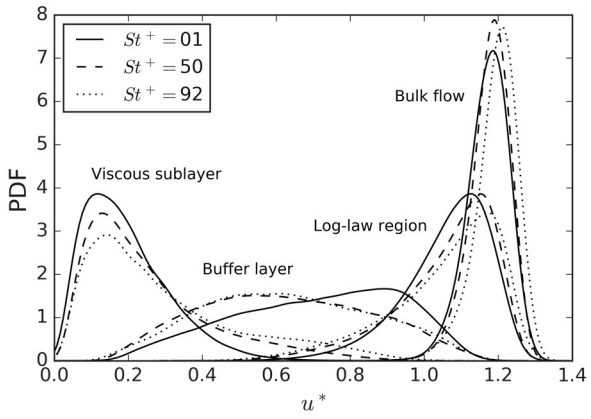

Figure 17: Effect of Stokes number on probability density functions of particle streamwise velocity in wall-normal channel regions.

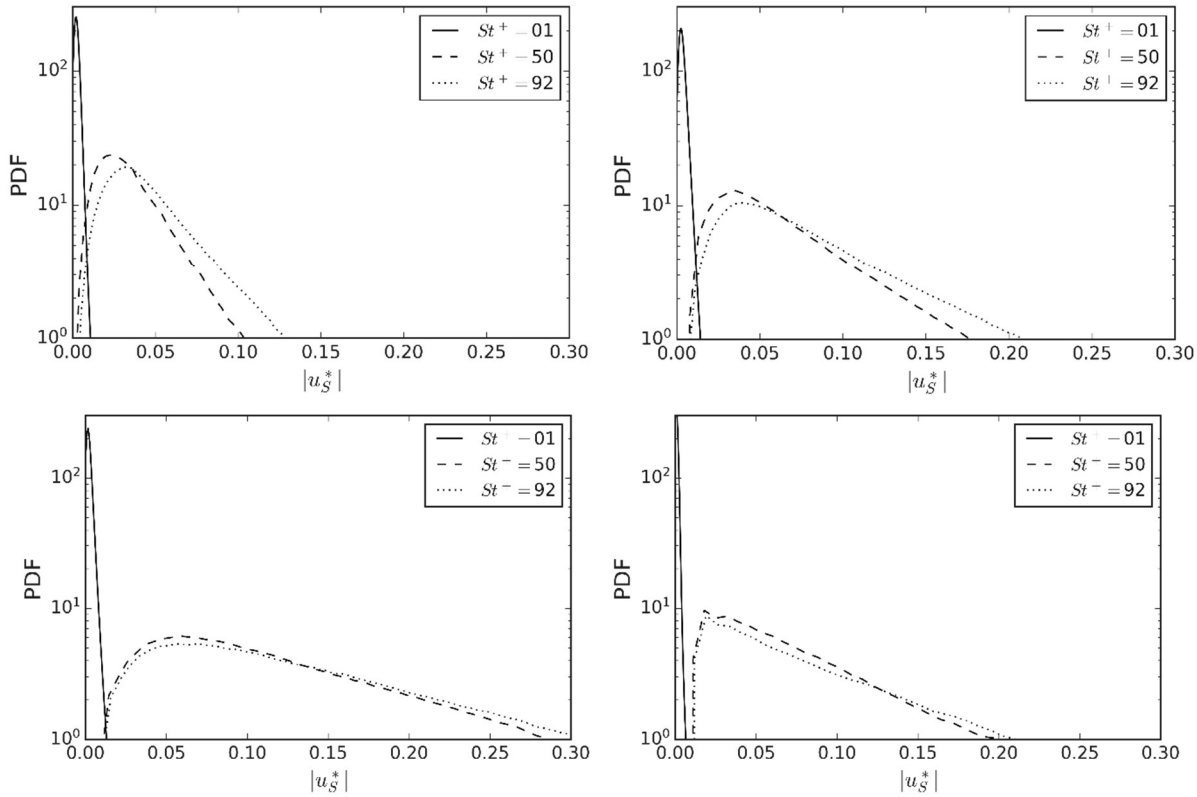

Figure 18: Effect of Stokes number on probability density functions of particle slip velocity in wall-normal channel regions. Upper left: bulk flow, upper right: log-law, lower left: buffer layer, lower right: viscous sublayer.

To further investigate this, and to relate back to the way in which coherent turbulent structures were observed to be altered in the previous subsection, the range of streamwise velocities in each wall-normal region of the channel flow is presented in Figure 17. Starting with the viscous sublayer, we observe that as the Stokes number is increased, the range of streamwise velocities present in that region increases significantly, hence it is likely that the coupling in the viscous sublayer will be strong. In the buffer layer, the two inertial particles sets exhibit similar profiles, with the tracer-like particles demonstrating skewing towards increased streamwise velocities. This may explain why in Figure 8 and Figure 12 both buffer-layer profiles exhibited similar modification from those representing the unladen flow. The low Stokes number particles show very little tendency to accumulate in low speed streaks within this region and so can retain their increased

velocity. It should also be mentioned that the distribution range across all Stokes numbers considered is very similar. As the bulk region of the channel is approached, the streamwise velocity distributions in all cases are comparable, with a slight skewing towards increased velocities for more inertial particles, in agreement with the results of Figure 16.

The distribution of slip velocities present in each wall-normal region is presented in Figure 18. The general trend with Stokes number persists throughout all regions of the channel, wherein the density ratio largely determines the maximum slip velocity as well as the spread, with the most inertial particles possessing the widest range of slip velocities. It is also evident that the largest slip velocity spreads are found in the buffer layer and the viscous sublayer, suggesting that these particles are the most decorrelated from the local flow field. This observation is in agreement with the most notable modifications to coherent turbulent structures observed in Figure 13.

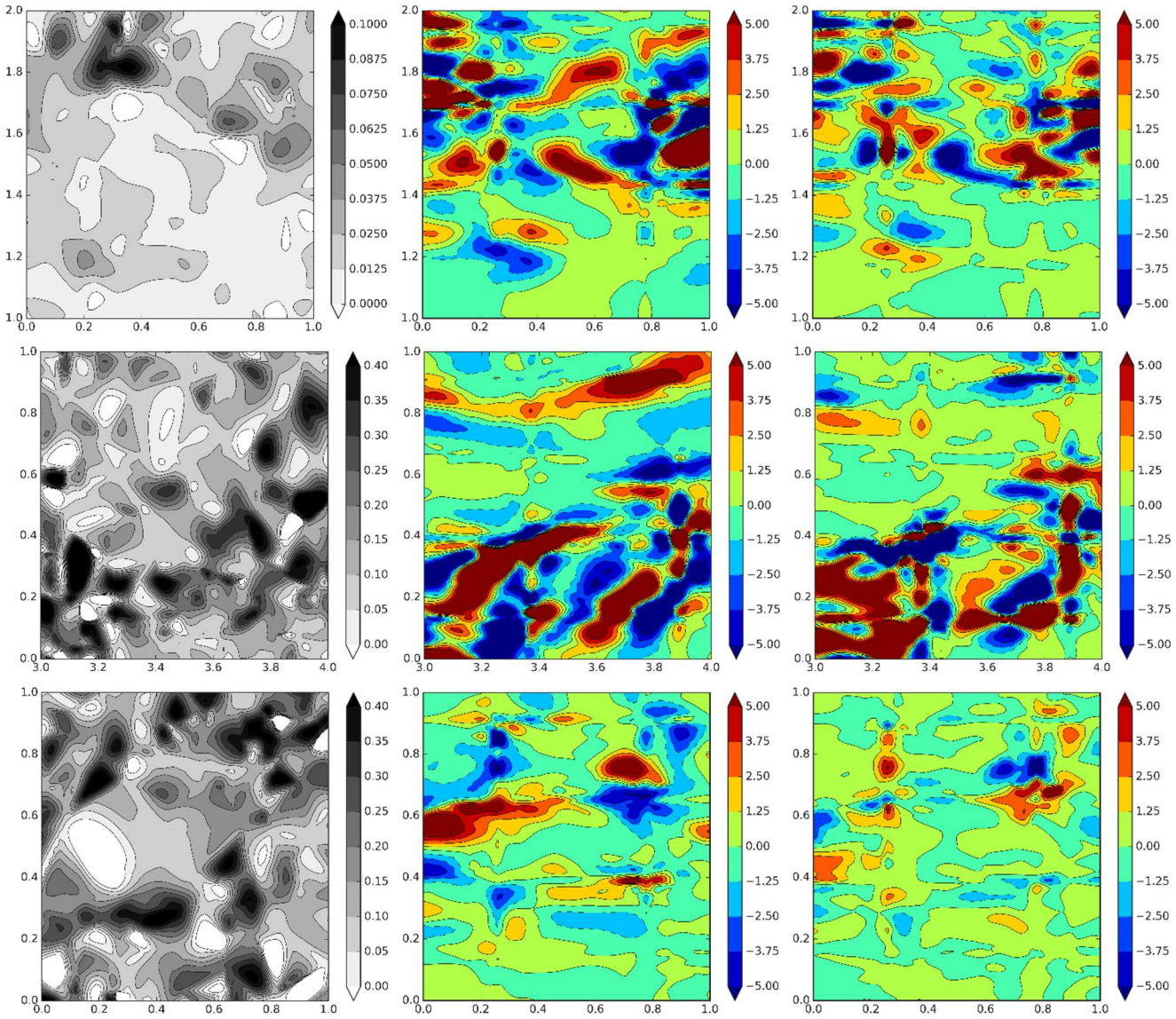

Figure 19: Effect of Stokes number on particle feedback force (left), Q (centre) and R (right). Upper: $St^+ = 0.1$, centre: $St^+ = 50$, lower: $St^+ = 92$. Slices taken in $x^* - z^*$ plane at $y^* = 0.1$.

The range of slip velocities as an indicator of the extent of coupling proves to be a suitable parameter for gauging the degree of turbulence modulation. The final part of the analysis shall focus on how the feedback force is distributed in the buffer layer, wherein the

strongest slip velocities were recorded, in an effort to understand the mechanisms surrounding how the turbulent structures are modified by the presence of the particles. The particle feedback force is presented along with the corresponding Q and R values in pseudocolour contour plots in Figure 19. In all three cases, it is evident that the PSIC feedback field is continuous and smooth. This is because for the two inertial particle species considered, the concentrations in the regions where the coupling is most prominent is sufficiently high. Furthermore, the present study employs a spectral element method approach to the continuous phase, which is function-based across an individual element rather than cell-based. Hence, the fluid solver applies to the source term the local element distribution of particle forces on each Gauss-Lobatto-Legendre point, before obtaining a function-based solution across the entire element. This means that the present method has less demanding requirements on the nature of the forcing field, unlike lower-order methods which use only a few neighbouring points to time-evolve each node. From Figure 19 we may also infer the particle size ($d_p^* = 0.005$) compared the associated length scales of turbulence structures, which possess a typical width of around 0.5δ. Hence, the particle size is on the order of 1% of the coherent turbulent structure, which is sufficiently small to resolve a smooth trajectory and hence force distribution across the scales of the structure.

The top row represents the tracer-like ($St^+ = 0.1$) particles which instantaneously exhibit comparatively lower coupling between the phases. In the middle plot, indicating Q, long streaks in orange/red represent slices through the cores of quasistreamwise vortices and there appears to be a trend in which the forcing is strongest surrounding these structures. The low but non-negligible slip velocity present around these structures clearly influences the surrounding fluid flow field. Specifically, the strongest coupling appears to be in the ejection region of the vortices between the high Q areas wherein particles are likely to lag the fluid flow. This produces large forces on low speed streaks located between the two structures which has previously been suggested to cause instabilities, leading to the generation of more quasistreamwise vortices (Jiménez and Pinelli, 1999). This influence helps to explain the frequency of increased Q regions, as observed in

Figure 7 and Figure 12. The midrange particles (centre) also exhibit the same increased feedback forces in between the Q-criterion satisfying regions. Previous work (Lee and Lee, 2015) suggests that particles entering these regions (which experience large deceleration due to the high slip velocity) accelerate the fluid in the low speed streaks thereby suppressing the generation of quasistreamwise vortices leading to being fewer present in the flow. Very large particle feedback can be observed in those regions in Figure 18, lending to the credibility of this explanation. Finally, at $St^+ = 92$, particle-fluid coupling in the buffer layer is sufficiently strong that both increased Q and R regions are very infrequent. In this case, the level of turbulence suppression is increased because, despite exhibiting less tendency to become trapped in these regions, particles migrating through low speed streaks exert even greater acceleration on the fluid.

IV. CONCLUSIONS AND OUTLOOK

This study has considered the effect of Stokes number, adjusted through the particle-fluid density ratio, on the modification of coherent turbulent structures within a particle-laden channel flow at $Re_\tau = 180$. To perform such, direct numerical simulation and Lagrangian particle tracking were performed to predict the trajectories and two-way particle-fluid interactions for three particle Stokes numbers, $St^+ = 0.1, 50$ and 92. Transition of the turbulence field upon injection of particles was monitored and an initial minima in the fluid velocity fluctuations within the first $t^* < 40$ was observed due to the response of the coupling term as the system adjusted to the presence of particles. This effect is often unreported in previous work and makes comparisons with similar studies difficult as simulations of this kind are often restricted to

short runtimes. The inclusion of the two-way coupling mechanism imparts significant differences to the turbulence field when compared to the unladen or one-way coupled flow. Analysis of the Eulerian statistics showed minor turbulence enhancement for the tracer-like particles, and turbulence suppression for the particles with increased density ratios. Furthermore, by considering Q-criterion isosurfaces, the frequency of quasistreamwise vortices close to the wall was increased by the tracer-like particles and reduced by the inertial particles. Our results indicate increased coupling forces in the regions surrounding these structures.

The structure of turbulence in the presence of particles was also shown to vary depending on wall-distance. Similar modifications to the distribution of Q were observed in the log-law region, with $St^+ = 50$ particles exhibiting very little influence on the distribution of Q. Both systems have similar streamwise root mean square velocity fluctuations and the extent of particle-fluid coupling effects correlates with this property. Invariants of the velocity gradient tensor, Q and R, indicated the greatest modification of coherent turbulent structures to be in the buffer layer and viscous sublayer. In both regions, the presence of $St^+ = 0.1$ particles widened the distribution of R, with the inertial particles causing the distribution of R to become narrower, meaning that the distribution was weighted more towards saddle point regions, reducing the amount of unstable focus / compressing regions and stable focus / stretching regions which account for the quasistreamwise vortices observed in these types of flow. Inertial particles in the viscous sublayer also cause a narrowing of the Q-R joint probability distribution function in the R direction, an observation which is missed by solely considering the Q-criterion as many papers adopt. The implications of a reduction in the spread of R is that the local flow field becomes more two-dimensional and laminar.

The inertial particles exhibited substantial turbophoresis over the time simulated, with the most migration towards the wall observed for the $St^+ = 50$ particles, which were also observed to preferentially concentrate in low speed streaks. It is also demonstrated that the particles surrounding these streaks have a wide range of velocities, which has consequences for the coupling field surrounding the quasistreamwise vortices which surround the low speed region. Particle root mean square velocity fluctuations increase with Stokes number in the streamwise direction, with the opposite trend true for the off-stream directions. From result this it is likely that the degree of coupling correlates more with streamwise velocity distributions, particularly for more inertial particles.

V. ACKNOWLEDGEMENTS

The authors are grateful for funding from the UK Engineering and Physical Sciences Research Council through the TRANSCEND (Transformative Science and Engineering for Nuclear Decommissioning) project (EP/S01019X/1).

VI. DATA AVAILABILITY

The data that support the findings of this study are available from the corresponding author upon reasonable request.

VII. REFERENCES

A. H. Abdelsamie and C. Lee. "Decaying versus stationary turbulence in particle-laden isotropic turbulence: Turbulence modulation mechanism." *Physics of Fluids.* **24**, 015106. (2012).

A. Aliseda, A. Cartellier, F. Hainaux and J. C. J. J. o. F. M. Lasheras. "Effect of preferential concentration on the settling velocity of heavy particles in homogeneous isotropic turbulence." **468**, 77-105. (2002).

M. Bernardini. "Reynolds number scaling of inertial particle statistics in turbulent channel flows." *Journal of Fluid Mechanics.* **758**, R1. (2014).

H. M. Blackburn, N. N. Mansour and B. J. Cantwell. "Topology of fine-scale motions in turbulent channel flow." *Journal of Fluid Mechanics.* **310**, 269-292. (1996).

M. Boivin, O. Simonin and K. D. Squires. "Direct numerical simulation of turbulence modulation by particles in isotropic turbulence." *Journal of Fluid Mechanics.* **375**, 235-263. (1998).

M. Boivin, O. Simonin and K. D. Squires. "On the prediction of gas–solid flows with two-way coupling using large eddy simulation." *Physics of Fluids.* **12**, 2080-2090. (2000).

J. W. Brooke, K. Kontomaris, T. Hanratty and J. B. McLaughlin. "Turbulent deposition and trapping of aerosols at a wall." *Physics of Fluids A: Fluid Dynamics.* **4**, 825-834. (1992).

M. S. Chong, A. E. Perry and B. J. Cantwell. "A general classification of three-dimensional flow fields." *Physics of Fluids A: Fluid Dynamics.* **2**, 765-777. (1990).

A. Daitche. "On the role of the history force for inertial particles in turbulence." *Journal of Fluid Mechanics.* **782**, 567-593. (2015).

M. De Marchis and B. Milici. "Turbulence modulation by micro-particles in smooth and rough channels." *Physics of Fluids.* **28**, 115101. (2016).

F. F. Dizaji and J. S. Marshall. "On the significance of two-way coupling in simulation of turbulent particle agglomeration." *Powder Technology.* **318**, 83-94. (2017).

J. K. Eaton. "Two-way coupled turbulence simulations of gas-particle flows using point-particle tracking." *International Journal of Multiphase Flow.* **35**, 792-800. (2009).

J. K. Eaton and J. Fessler. "Preferential concentration of particles by turbulence." *International Journal of Multiphase Flow.* **20**, 169-209. (1994).

S. Elghobashi. "Particle-laden turbulent flows: direct simulation and closure models." *Applied Scientific Research.* **48**, 301-314. (1991).

S. Elghobashi. "On predicting particle-laden turbulent flows." *Applied Scientific Research.* **52**, 309-329. (1994).

S. Elghobashi. "An Updated Classification Map of Particle-Laden Turbulent Flows." In: *IUTAM Symposium on Computational Approaches to Multiphase Flow: Proceedings of an IUTAM Symposium held at Argonne National Laboratory, October 4-7, 2004*: Springer Science & Business Media, 3. (2007).

M. Fairweather and J.-P. Hurn. "Validation of an anisotropic model of turbulent flows containing dispersed solid particles applied to gas–solid jets." *Computers & Chemical Engineering.* **32**, 590-599. (2008).

A. Ferrante and S. Elghobashi. "On the physical mechanisms of two-way coupling in particle-laden isotropic turbulence." *Physics of Fluids.* **15**, 315-329. (2003).

P. F. Fischer, J. W. Lottes and S. G. Kerkemeier. 2008. *Nek5000.* [Online]. [Accessed 1st September]. Available from: http://nek5000.mcs.anl.gov

R. A. Gore and C. T. Crowe. "Effect of particle size on modulating turbulent intensity." *International Journal of Multiphase Flow.* **15**, 279-285. (1989).

J. C. Hunt, A. A. Wray and P. Moin. "Eddies, streams, and convergence zones in turbulent flows." *Center for Turbulence Research Report CTR-S88.* (1988).

J. Jiménez and A. Pinelli. "The autonomous cycle of near-wall turbulence." *Journal of Fluid Mechanics.* **389**, 335-359. (1999).

M. H. Kasbaoui, D. L. Koch and O. J. J. o. F. M. Desjardins. "The rapid distortion of two-way coupled particle-laden turbulence." **877**, 82-104. (2019).

J. Kuerten and A. Vreman. "Can turbophoresis be predicted by large-eddy simulation?" *Physics of Fluids.* **17**, 011701. (2005).

J. D. Kulick, J. R. Fessler and J. K. Eaton. "Particle response and turbulence modification in fully developed channel flow." *Journal of Fluid Mechanics.* **277**, 109-134. (1994).

J. Lee and C. Lee. "Modification of particle-laden near-wall turbulence: Effect of Stokes number." *Physics of Fluids.* **27**, 023303. (2015).

Y. Li, J. B. McLaughlin, K. Kontomaris and L. Portela. "Numerical simulation of particle-laden turbulent channel flow." *Physics of Fluids.* **13**, 2957-2967. (2001).

J. L. Lumley. "Drag reduction in turbulent flow by polymer additives." *Journal of Polymer Science: Macromolecular Reviews.* **7**, 263-290. (1973).

K. Luo, Z. Wang, D. Li, J. Tan and J. Fan. "Fully resolved simulations of turbulence modulation by high-inertia particles in an isotropic turbulent flow." *Physics of Fluids.* **29**, 113301. (2017).

M. Maxey. "The motion of small spherical particles in a cellular flow field." *The Physics of Fluids.* **30**, 1915-1928. (1987).

M. R. Maxey and J. J. Riley. "Equation of motion for a small rigid sphere in a nonuniform flow." *Physics of Fluids.* **26**, 883-889. (1983).

R. Monchaux and A. J. P. R. F. Dejoan. "Settling velocity and preferential concentration of heavy particles under two-way coupling effects in homogeneous turbulence." **2**, 104302. (2017).

L. F. Mortimer, D. O. Njobuenwu and M. Fairweather. "Near-wall dynamics of inertial particles in dilute turbulent channel flows." *Physics of Fluids.* **31**, 063302. (2019).

Y. Pan and S. Banerjee. "Numerical simulation of particle interactions with wall turbulence." *Physics of Fluids.* **8**, 2733-2755. (1996).

M. Picciotto, C. Marchioli and A. Soldati. "Characterization of near-wall accumulation regions for inertial particles in turbulent boundary layers." *Physics of Fluids.* **17**, 098101. (2005).

L. M. Portela, P. Cota and R. V. Oliemans. "Numerical study of the near-wall behaviour of particles in turbulent pipe flows." *Powder Technology.* **125**, 149-157. (2002).

P. K. Ptasinski, B. J. Boersma, F. T. M. Nieuwstadt, M. A. Hulsen, B. H. A. A. Van Den Brule and J. C. R. Hunt. "Turbulent channel flow near maximum drag reduction: simulations, experiments and mechanisms." *Journal of Fluid Mechanics.* **490**, 251-291. (2003).

A. K. Pukkella, R. Vysyaraju, V. Tammishetti, B. Rai and S. Subramanian. "Improved mixing of solid suspensions in stirred tanks with interface baffles: CFD simulation and experimental validation." *Chemical Engineering Journal.* **358**, 621-633. (2019).

J. J. Riley and G. Patterson Jr. "Diffusion experiments with numerically integrated isotropic turbulence." *The Physics of Fluids.* **17**, 292-297. (1974).

C. B. Rogers and J. K. Eaton. "The effect of small particles on fluid turbulence in a flat-plate, turbulent boundary layer in air." *Physics of Fluids A: Fluid Dynamics.* **3**, 928-937. (1991).

D. W. Rouson and J. K. Eaton. "On the preferential concentration of solid particles in turbulent channel flow." *Journal of Fluid Mechanics.* **428**, 149-169. (2001).

G. Sardina, P. Schlatter, L. Brandt, F. Picano and C. M. Casciola. "Wall accumulation and spatial localization in particle-laden wall flows." *Journal of Fluid Mechanics.* **699**, 50-78. (2012).

Y. Tsuji, Y. Morikawa and H. Shiomi. "LDV measurements of an air-solid two-phase flow in a vertical pipe." *Journal of Fluid Mechanics.* **139**, 417-434. (1984).

B. van Wachem, M. Zastawny, F. Zhao and G. Mallouppas. "Modelling of gas–solid turbulent channel flow with non-spherical particles with large Stokes numbers." *International Journal of Multiphase Flow.* **68**, 80-92. (2015).

B. Vreman, B. J. Geurts, N. Deen, J. Kuipers and J. G. Kuerten. "Two-and four-way coupled Euler–Lagrangian large-eddy simulation of turbulent particle-laden channel flow." *Flow, Turbulence and Combustion.* **82**, 015102. (2009).

C. Winkler, S. L. Rani and S. Vanka. "Preferential concentration of particles in a fully developed turbulent square duct flow." *International Journal of Multiphase Flow.* **30**, 27-50. (2004).

Z. Wu and Y. Cao. "Numerical simulation of airfoil aerodynamic performance under the coupling effects of heavy rain and ice accretion." *Advances in Mechanical Engineering.* **8**, 1687814016667162. (2016).

Z. Zhang and Q. Chen. "Comparison of the Eulerian and Lagrangian methods for predicting particle transport in enclosed spaces." *Atmospheric Environment.* **41**, 5236-5248. (2007).

F. Zhao, W. George and B. Van Wachem. "Four-way coupled simulations of small particles in turbulent channel flow: The effects of particle shape and Stokes number." *Physics of Fluids.* **27**, 083301. (2015).

L. Zhao, H. I. Andersson and J. Gillissen. "Turbulence modulation and drag reduction by spherical particles." *Physics of Fluids.* **22**, 081702. (2010).

L. Zhao, H. I. Andersson and J. J. Gillissen. "Interphasial energy transfer and particle dissipation in particle-laden wall turbulence." *Journal of Fluid Mechanics.* **715**, 32-59. (2013).

R. Zisselmar and O. Molerus. "Investigation of solid-liquid pipe flow with regard to turbulence modification." *The Chemical Engineering Journal.* **18**, 233-239. (1979).